Hierarchical Porous Recycled PET Nanofibers for High-Efficiency Aerosols and Virus Capturing

DOI:
10.1021/acsami.1c17157

Document Version
Accepted author manuscript

Article Id: am1c17157

Hierarchical ~~porous recycled-PET nano-fibers~~ Porous Recycled PET Nanofibers for ~~high efficiency aerosols~~ High-Efficiency Aerosols and ~~virus capturing~~Virus Capturing

Jun~~-~~ Song, Qi~~-~~ Zhao, Chen~~-~~ Meng, Jinmin~~-~~ Meng, Zhongda~~-~~ Chen, Jiashen~~-~~ Li~~*~~;

Department of Materials, The University of Manchester, Manchester~~,~~ M13 9PL, ~~UK~~U.K.

~~*-~~ ~~E-mail:~~Email: jiashen.li@manchester.ac.uk.

29-09-2021

Abstract

Plastic crisis, especially for ~~polyethylene terephthalate~~poly(ethylene terephthalate) (PET) bottles, has been one of the greatest challenges for the earth and human beings. Processing ~~recycled-PET~~ recycled PET (rPET) into functional materials has the dual significance of both sustainable development and economy. Providing more possibilities for the engineered application of rPET, porous PET fibers can further enhance the high specific surface area of electrospun membranes. ~~Here~~Here, we use a two-step strategy of electrospinning and ~~post-processing~~postprocessing to successfully control the surface morphology of rPET fibers. Through a series of optical and thermal characterizations, the porous morphology formation mechanism and crystallinity induced by solvents of rPET fibers ~~was~~were discussed. Then, this work further investigated both PM2.5 air pollutants and protein filtration performance of rPET fibrous membrane. The high capture capability of rPET membrane demonstrated its potential application as an integrated ~~high-efficiency~~ high-efficiency aerosol filtering solution.

Keywords

waste bottle; electrospinning; porous fiber; ~~polyethylene terephthalate~~poly(ethylene terephthalate) (PET); air filtration

1~~.~~. Introduction

Graphic abstractCorresponding ~~author's~~author'sSupporting InformationAuthor InformationCorresponding AuthorJiashen Li - Department of Materials, The University of Manchester, Manchester, M13 9PL, UK; http://orcid.org/0000-0001-7333-5280; Email: jiashen.li@manchester.ac.ukAuthorsJun Song - Department of Materials, The University of Manchester, Manchester, M13 9PL, UK; https://orcid.org/0000-0002-7689-1722Qi Zhao - Department of Materials, The University of Manchester, Manchester, M13 9PL, UK; https://orcid.org/0000-0002-9193-628XChen Meng - Department of Materials, The University of Manchester, Manchester, M13 9PL, UK; https://orcid.org/0000-0001-5540-553XJinmin Meng - Department of Materials, The University of Manchester, Manchester, M13 9PL, UK; https://orcid.org/0000-0003-1471-7531Zhongda Chen - Department of Materials, The University of Manchester, Manchester, M13 9PL, UK; https://orcid.org/0000-0003-0518-7938Declaration of Competing InterestThe authors declare that they have no known competing financial interests or personal relationships that could have appeared to influence the work reported in this paper.Data AvailabilityTable of Contents (TOC)The United Nations sustainable development goals are committed to being carbon neutral on earth.[1] As the major carbon emission states, China, the European ~~Union~~Union, and the United States ~~are~~have proposed their roadmaps ~~towards~~toward more sustainable economies.[2] Food and beverage packaging is an indispensable part of modern lifestyle and economies. However, the current disposal of beverage plastic bottles made from PET has been a serious concern for decades due to their massive pollution on the environment and human beings, though an alternative sustainable roadmap is promoting biodegradable plastic bottles and packages.[3,4] Furthermore, the demand for personal ~~protect~~protective equipment (PPE, including protective suit, face ~~masks,~~mask, face shield), which is superimposed on the global spread of the COVID-19 epidemic, remains high.[5] The supply chain and sustainable recycling of polymetric plastic raw materials have become urgent problems in the very near future.

Recycled PET (rPET) has been widely used in the textile industry to produce ~~non-woven~~nonwoven fabrics, garments, ~~ropes~~ropes, and other chemical engineering materials. Therefore, the investigation of recycled engineering is ~~not only~~ a solution not only to the sustainable ~~development,~~development but also for improving the value ~~to~~of PET products.

Electrospinning is a facile technology to produce fibers with ~~nano/micro scales~~ nano/microscales in quantity. Although the ~~non-woven~~nonwoven membranes stacked by the electrospun fibers have a large number of voids and holes, these fibrous membranes could not be regarded as porous electrospun fibers.[6] Porous fibers should refer to the pits or voids on the surface or interior of the individual single fiber. Combining with the holes on electrospun nonwoven membranes, such materials can be considered as hierarchical porous fibers. Hierarchical porous electrospun fibers show advantages in a variety of applications including tissue engineering,[7] protective and smart ~~clothing~~clothing, and filtration due to their higher specific surface area and roughness interfaces.[8,9] For ~~instances,~~instance, hierarchical porous fibrous membranes have more contact area to intercept pollutant particles in gas medium and to load more pollutants.[10,11] The ~~micro-hierarchy~~ microhierarchy structures can also mimic human extracellular matrix and elevate cell attachment and proliferation performances.[12]

~~Conventional~~ The conventional porous formation mechanism for electrospinning process is similar to the template casting fabrication.[13] The formation of pores during electrospinning is essentially a process of controlling the solidification of the polymer from the solution. According to the strategy of the curing process, the porous formation mechanisms at this stage can be divided into ~~thermal-induced~~ thermal-induced phase separation (TIPS) that ~~involving~~involves temperature ~~changing, solvent-induced~~ changes, solvent-induced phase separation (SIPS) that selects a highly volatile solvent, or ~~non-solvent-induced~~ non-solvent-induced phase separation (NIPS) that applies diffusive exchange with a ~~non-solvent~~nonsolvent during spinning or casting.[14] Specifically, most ~~of~~ researchers have generally accepted in recent years that the trifluoroacetic acid ~~(TFA)/ dichloromethane~~ (TFA)/dichloromethane (DCM) solvent system is the mainstream choice for electrospinning PET fibers though the specific solution ratios were different.[15–17] However, this choice can only prepare conventional smooth fibers. As a case of SIPS, Shu et al. reported PET fibers with some pits on the surface by applying hexafluoro isopropanol (HFIP)/ DCM solution systems under a ~~high-humidity (60%–80%)~~ high-humidity (60–80%) environment.[18] The precise and universal parameters for fabricating porous rPET fibers are worthy to be studied. Previous publications have repeatedly proved that these ~~o f~~ pores formed during electrospinning are often ~~unform~~uniformly distributed, and the improvement of the ~~fiber's~~fiber's specific surface area is limited.

The majority of macromolecular electrospun fibers are in a low-crystalline or ~~non-crystalline~~noncrystalline state.[15] Therefore, organic solvent ~~system-induced re-crystallization~~ system-induced recrystallization of macromolecules is an alternative to modify ~~fiber's~~fiber's hierarchical porous surface morphology after electrospinning. The ~~recent~~recently published systematic research has successfully implemented this theory on PLLA fibers.[19] rPET is a ~~co-polymer~~ copolymer that can ~~be induced re-crystallization~~ induce recrystallization by solvents.[20] In view of the dissolution characteristics of PET, the careful selection of solvent systems to swell polymers rather than dissolve them is the key to the successful fabrication of porous electrospun PET fibers. The selected solvent systems would enter the rPET fiber ~~interior~~interior, where the NIPS mechanism ~~formed~~ takes place during the electrospinning.

In this article, we used a conventional spinning solution at room environment that followed ~~by~~ a novel post-treatment strategy to prepare hierarchical porous rPET fibers. The crystalline and ~~the~~ porous surface of PET fibers can be controlled through adjusted parameters of the solvent system. The parameters of electrospinning preparation were ~~confirmed, while the~~ confirmed during post-treatment, i.e., a variety of solution systems for solvent-induced recrystallization have been designed and implemented. Subsequently, the surface morphology, solvent residue, thermophysics, and the crystallinity of rPET fibers were characterized. The mechanism of hierarchical porous formation was discussed on account of characterization data. Finally, the PM2.5 and virus filtration performances of electrospun rPET fibrous membrane were evaluated.

2.~~.~~ Materials and ~~methods~~Methods

2.1.~~.~~ Materials

The rPET used in this study was ~~Coca-Cola®~~Coca-Cola coke plastic bottles ~~which~~that were sold in a UK grocery. TFA, acetone, and ethanol were purchased from Alfa Aesar, ~~UK.~~U.K. DCM and ~~N-Methyl-2-pyrrolidone (NMP)were~~ -methyl-2-pyrrolidone (NMP) were purchased from ~~Sigma-Aldrich, USA.~~Sigma-Aldrich.

2.2.~~.~~ Electrospinning and ~~post-treatment~~Post-Treatment

~~Electrospun~~Electrospinning and the consequent post-treatment ~~for~~ process of rPET ~~were~~are demonstrated in Figure 1. rPET bottles were

shredded into small pieces about 5 ~~×~~× 5 mm^2 after ~~rinsed~~rinsing with ethanol. PET pieces were dissolved by a dual-solvent system that was mixed by TFA and DCM by 1:1 ratio by weight. The PET electrospun solution (10% w/w) could be obtained after ~~a 24 h~~24 h stirring at room temperature. TONG LI TECH Nanofiber Electrospinning Unit (Shenzhen, China) was used to produce an rPET ~~nano-fibrous~~nanofibrous membrane at 25 ~~°C~~°C and 40% humidity. The PET/TFA/DCM spinning solution ejection feeding rate was 1 ~~ml/h,~~mL/h, while the receiving distance and supply voltage from electrospinning needle tip to drum collector were 25 cm and 15 kV, respectively. All sample groups were dried in a fume hood for 24 h before further processing to ensure the complete evaporation of organic solvents.

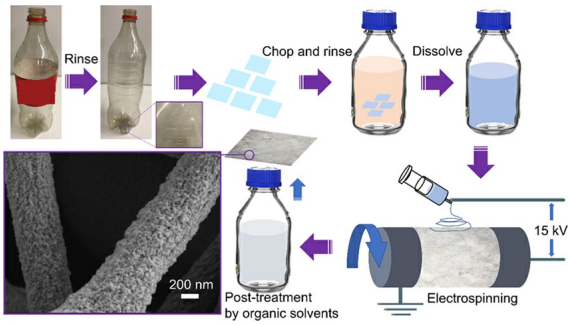

1~~.~~. ~~The schematic~~ Schematic diagram of recycled PET electrospinning and post-treatment process.

The PET fibrous membranes were immersed ~~into~~in different organic solvents for 30 ~~mins~~min as post-treatment. The specific design of experiments ~~was~~is shown in Table 1. For specimens after NMP/ethanol treatment, they were rinsed with ethanol absolute twice, 5 min each time to remove NMP solvent inside the fibrous membrane interior. All rPET specimens after solvent post-treatment were dried in the fume board at room temperature ~~for~~ overnight before further experimental analysis, to ensure the complete evaporation of the solvent in the samples.

1~~.~~.

Design of ~~experiments~~Experiments for ~~electrospun~~Electrospun rPET ~~fibrous membranes~~Fibrous Membranes

~~Sample~~sample ID	~~Post-treatment~~post-treatment solvents ~~(w/w)~~(w/w)	~~Temperature (°C)~~temperature (°C)
A	~~Acetone~~acetone	25
E	~~Ethanol~~ethanol	25
N1	~~NMP/ethanol~~NMP/ethanol ~~(50%:50%)~~(50:50%)	25
N2	~~NMP/ethanol~~NMP/ethanol ~~(37.5%:62.5%)~~(37.5:62.5%)	25
N3	~~NMP/ethanol~~NMP/ethanol ~~(25%:75%)~~(25:75%)	25
N4	~~NMP/ethanol~~NMP/ethanol ~~(50%:50%)~~(50:50%)	~~−20~~−20

2.3~~.~~. Characterizations

~~Surface~~ The surface morphology of PET fibers ~~were~~was observed by a field emission scanning electron ~~microscopies~~microscope (FE-SEMs, Philips XL30, The Netherlands, and Zeiss Ultra55, Germany) after platinum coating.

Fourier-transform infrared (FT-IR) spectroscopy was conducted by a Nicolet 5700 FT-IR ~~Spectrometer (Thermo, USA)~~ spectrometer (Thermo) with an attenuated total reflectance (ATR) smart orbit attachment. Different scanning calorimetry (DSC) was performed using Q1000 (TA ~~Instrument, USA),~~ Instruments), under a nitrogen (N_2) flow, with a heating rate of 8 ~~°C/min~~°C/min from 30 to 300 ~~°C.~~°C. Each group of specimens has three samples. X-ray diffraction (XRD) was operated on ~~a X'Pert~~an X'Pert Pro X-ray diffractometer (Panalytical, ~~UK)~~U.K.). The angle range was ~~from 3° to 70°.~~ 3–70°. The step size was about ~~0.033°~~0.033°. The time per step was set at 215 ~~seconds~~s.

The mechanical properties of pristine and NMP-treated rPET fibrous membrane were characterized by an Instron tensile tester (3344, ~~MA USA)~~ MA) with a ~~10N~~ 10 N load cell. The rPET fibrous membrane specimens were cut into 5 ~~×~~× 47 mm^2 and tested at room temperature with a displacement rate of 2 mm/min. Both groups of rPET fibrous membrane had three specimens for testing. The ~~Young's~~Young's modulus of fibrous membranes was calculated based on the obtained ~~stress-strain~~stress–strain curves.

2.4. Air filtration performance evaluation Filtration Performance Evaluation

2.4.1. PM2.5 aerosols filtration Aerosol Filtration

An rPET fibrous membrane was fixed on a 3D-printed 10 cm diameter round holder with a ducted fan driven by a brushless motor in a 100-liter 100-l storage box (Argos, UK) U.K.) as the confined room (Figure Figures 2a and S1). When the air flow is 3 m/s, the air flux through the membrane and holder is ~ 350 ~350 dm^3/min because the inner diameter of ducted fan is 5 cm. The pristine and NMP post-treated electrospun rPET fibrous membrane were used for comparing the filtration efficiency of fibers with different surface morphology. morphologies. Three groups of both pristine and NMP post-treated were selected with different membrane thickness thicknesses (Table S1 in the Supporting Information) by controlling the spinning time from 1 h to 3 h.

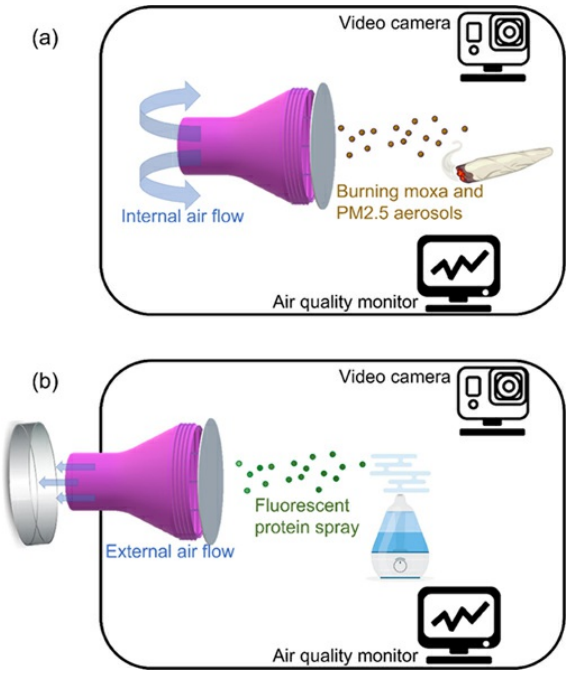

2. The schematic Schematic diagrams of air filtration tests: (a) internal air flow for PM2.5 aerosol capturing test, test and (b) external air flow for virus interception test.

Moxa is a traditional Chinese medicine which that could be burnt and burned to release a smoke contains containing inhalable particles, carbon monoxide, carbon dioxide, and volatile organic compounds.[21] Thus, moxa haze could mimic urban aerosol pollutants. A 0.05 g moxa stick (Changzhou, China) was burn for generating burned to generate PM2.5 aerosols. The high-speed airflow air flow motivated by the ducted fan continuously pushes the air to go through the filter membrane, membrane so that the aerosol particles in the confined space begin to accumulate on the membrane during the filtration test process as shown in Figure 2a. The downtrend of PM2.5 concentration (μg/m (μg/m^3) was recorded by an air quality monitoring system.

2.4.2. Virus spray filtration Spray Filtration

The green fluorescent protein monoclonal antibody (eGFP, Invitrogen, USA) Invitrogen) was used to mimic virus due to its availability of for further observation.[22] The eGFP was diluted and generated to to generate a mist spray that is sprayed by a household humidifier. The same 3D-printed membrane holder, holder and the ducted fan were used to draw the air from the box to the outside. When the air flow flows across the rPET fibrous membrane, the eGFP would be intercepted by the fibers as shown by Figure Figures 2b and S2. The petri Petri dish was placed behind the fan outside the box. The phase contrast light microscopy (Zeiss, Germany) was used to observe the eGFP on the fibrous membrane membrane, and petri a Petri dish was used for investigating the filtration performance of pristine and NMP post-treated electrospun PET membranes. The second (electret nonwoven) and third (contact face) layers of commercial surgical face mask (TG, UK EN14683:2019) were used as the control group.

2.5. Software

Electrospun rPET fiber diameters, diameters and mechanical properties were collected determined by applying Image J (version 1.8.0, NIH,

USA). NIH). The results of fiber diameter were presented as means ±mean ± standard deviations.deviation.

3. Results and discussionsDiscussion

3.1. Surface morphologyMorphology

3.1.1. Surface morphologyMorphology of electrospunElectrospun rPET fibersFibers

Figure 3 shows the surface morphology of pristine electrospun PET fibers under 20,00020000 magnifications. The fibers were randomly oriented. Although most of fibers had smooth surface and round shape, there were few bead fibers were observed. It could be attributed to the relatively low polymer concentration. With the fast evaporation of DCM in PET electrospinning solution, the lower solution concentration leadedled to a lower solution viscosity, which was not able to form thin fibers with a higher specific area.

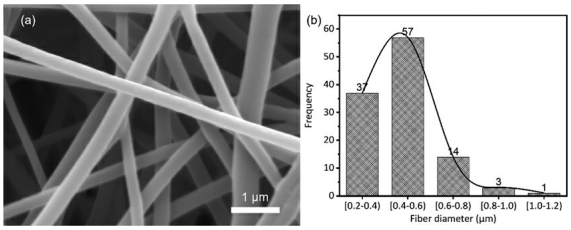

3. (a) SEM images of pristine electrospun rPET fibers,fibers and (b) rPET fiber diameter counts.

It could also be observed that the fibers were adhered with each other, which can be attributed to the slow evaporation of TFA due to its relatively high boiling point (72 °C)°C) and low vapor pressure (97.5 mmHg, 20 °C).°C). The fibers might collapse and were interconnected with each other interconnect before TFA was completely evaporated. Furthermore, the relatively lower PET concentration of spinning solution also led to the fibers' adhesion.adhesion of fibers.[23] The lower PET concentration resulted in thinner fiber diameters, which were more likely to collapse and connect with each other. The most Most of PET fibers (83.9%) were in the size range from 0.2 μm to 0.6 μm. of 0.2–0.6 μm. The average diameter of electrospinning PET solution at a concentration of 10 wt% wt % was 0.48 ±± 0.15 μm. Comparingμm. Compared with previous studies, it could be found the different ratioratios of TFA/DCM solution systems maybe effectmay affect the fiber diameter. Significantly differing with thatdifferent from those of TFA (42.1 and 13.4 ××10^{-3} J*m^{-2}), DCM has a lower dielectric constant and a higher surface tension (8.9 and 27.2 ××10^{-3} J*m^{-2}). The morehigher DCM volume in the electrospinning solution can decrease the stretching of the polymer flow jet during the electrospinning process, then leadedwhich led to the larger electrospun fiber diameters. As a critical scenario of NIPS, the different solubilitysolubilities and volatilization ratesrates of TFA and DCM make a certain gap between the surface of the fiber and the PET molecular chain interior, which provides the possibility for subsequent solvent-induced recrystallization.

3.1.2. Surface morphologyMorphology of post-treatedPost-Treated PET fibersFibers

Figure 4 shows the SEM images forof electrospun rPET fibers after different solvents treatment under 10,00010000 magnifications. The immersing duration, 30 min, was same for all specimens treated by different solvents. The recipes for different solvent systems are illustrated in Table 1. The surface of ethanol treated ethanol-treated PET fibers (Figure 4a) became a little rougher than pristine fibers. By contrast, the fibers treated by acetone (Figure 4b) or NMP/ethanol (Figure 4c–f)c–f) had a completely different surface morphology.morphologies. The surface of acetone treated acetone-treated fibers was much rougher than ethanol treated that of ethanol-treated and pristine fibers. The rough surface of NMP/ethanol treated NMP/ethanol-treated PET fibers had some tiny voids. Therefore, the porous structure on the surface of fibers treated with NMP/ethanol should increase their surface area compared with pristine electrospun PET fibers. However, the pore sizes range from micrometer among adjacent fibers to nanometer inside individual fibers. Therefore, it is difficult to reveal the overall porous structure and surface area by a single method, e.g.e.g., pressurized mercury method and N_2 absorption method.

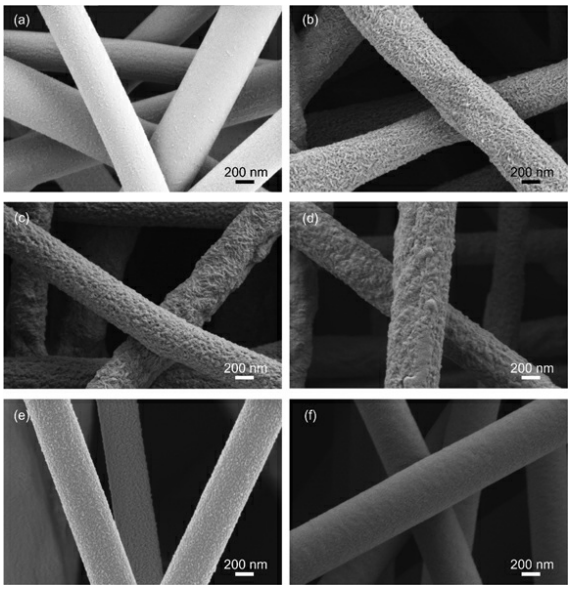

4~~.~~ . SEM images of rPET fibers treated by different solvents for 30 min. (a) ~~ethanol~~Ethanol absolute; (b) acetone; (c) NMP/ethanol, (1:1 ~~wt%);~~ wt %); (d) NMP/ethanol, (1:1 ~~wt%)~~ wt %) after ethanol resin; (e) NMP/ethanol, (3:5 ~~wt%);~~ wt %); and (f) NMP/ethanol, (1:3 ~~wt%).~~ wt %).

The different parameters of these solvents (Table 2) resulted in ~~the~~ different ~~morphology~~morphologies of rPET fibers after solvent post-treatment. These post-treatment solvents were carefully selected with the comprehensive consideration of their boiling point, viscosity, volatility, and, most importantly, solubility to the PET molecule. As an improved quantitative strategy for ~~"like~~"like dissolves ~~like",~~like", solubility parameter is a widely acknowledged theoretical model for evaluating the specific solubility between polar molecular polymers and solvent.[24] Hansen solubility parameters ~~is a criterion that composed of three variables including~~ include molecular dispersion, ~~polar~~polar, and ~~hydrogen-bonding~~hydrogen bonding.[25] Hildebrand solubility parameters can be considered as the vector sum of these three variables. The closer the Hildebrand solubility parameters of polymer and solvent are, the more likely they are to dissolve.

2~~.~~ .

Properties of ~~solvents used~~Solvents Used in ~~this study [boiling point; dielectric constant (ε); surface tension; viscosity (η);~~This Study [Boiling Point; Dielectric Constant (ε); Surface Tension; Viscosity (η); Hildebrand ~~solubility parameter (δ); vapor pressure]~~Solubility Parameter (δ); Vapor Pressure]

~~Solvent~~solvent	~~Boiling~~boiling point ~~(°C)~~(°C)	~~Dielectric~~dielectric constant ~~(ε)~~(ε)	~~Surface~~surface tension ~~(J/m~~(J/m^2)~~^{2})~~	~~Viscosity (η,~~viscosity (η, mPa·s~~mPa·s)~~)	Hildebrand ~~Solubility Parameter (~~solubility parameter (MPa$^{1/2}$)~~*MPa*$^{1/2}$)~~	~~Vapor~~vapor pressure (mmHg, 20 °C~~20 °C)~~)
TFA	72	42.1	0.13	0.93	10.8	97.5
DCM	39.7	9.1	0.27	0.45	4.9	354.8
~~Ethanol~~ethanol	78.3	24.3	0.02	1.20	13.2	44.6
~~Acetone~~acetone	56.1	20.6	0.02	0.31	9.9	184
NMP	203	33	0.41	1.65	11.4	0.3

The solubility parameters between NMP and PET ~~was relative~~were relatively narrow. NMP is the mainstream post-treatment solvent for PET,[26] while acetone is a typical highly polar solvent. The PET fibers would be swollen during ~~immersing~~immersion in the NMP/ethanol solvents and the NMP ~~solvent induced re-crystallization happened.~~ solvent-induced recrystallization occurred. Along with the movements of PET molecular chains during ~~forming crystal,~~crystal formation, solvents were squeezed out of the crystallization part of fibers and phase separation ~~happens~~occurs. Due to the high boiling point (202 ~~°C),~~°C), the evaporation rate of NMP was ~~pretty~~ low. The interaction between NMP and PET fibers was strong. It is thus held that the morphology and other properties of fibers after NMP/ethanol treatment might change gradually before ~~totally~~total evaporation of NMP. The specimens treated by NMP/ethanol were rinsed by ethanol with a high evaporation rate for obtaining reliable and consistent results. After ethanol ~~evaporating,~~evaporation, porous PET fibers were formed.

By contrast, ethanol has a far different solubility parameter ~~with~~from PET, which means that it is a bad solvent for the PET molecule.

Therefore, the PET ~~re-crystallization~~recrystallization would not happen during ~~immersing~~immersion in ethanol absolute, nor significant morphological changes of rPET fibers was observed.

~~Amorphous~~ The amorphous PET film could be swollen and ~~became crystallinity~~become crystalline in ~~the~~ acetone at 25 ~~°C.~~°C.[27] As a result, the ~~morphology~~morphological changes of rPET fibers after post-treatment by acetone might be attributed to the ~~swollen~~swelling and ~~re-crystallization~~recrystallization during the ~~immersing.~~immersion. However, there ~~were~~was only ~~roughness~~ a rough surface instead of voids or pores on PET fibers after acetone ~~post-treated.~~post-treatment. The possible reason was that the PET experienced the first stage of crystallization during ~~immersing~~immersion in acetone for 30 ~~minutes~~min at 25 ~~°C~~°C, and no voids appeared during this process.[28] ~~Acetone induced re-crystallization~~The acetone-induced recrystallization process could change the morphology of PET fiber ~~membranes~~membranes, and the ~~fibers'~~fibers' surface would ~~turned into~~ become rougher than that of pristine electrospun fibers.[29]

Figure 4 also compares rPET fibers after post-treatment with ~~different ratio~~ NMP/ethanol ~~solvents.~~ solvents of different ratios. In general, the surface ~~morphology~~morphological changes became invisible with ~~the~~ decreasing amount of NMP in the treatment mixture. Ethanol had limited interaction with PET due to ~~their~~its Hansen solubility parameters. The morphological changes would not happen when ~~fibers~~ immersing fibers in ~~the~~ pure ethanol. As a result, the penetration ability of the solvent mixture was limited when ethanol is the dominant solvent in the mixture. PET fibers would not ~~swell~~swell, and thus ~~re-crystallization~~recrystallization of PET was relatively low, which resulted in a limited ~~morphology~~morphological change of the PET fiber surface. As for temperature, the ~~morphology~~morphological changes after immersing in NMP/ethanol 50:50 mixtures became less significant as the immersing temperature decreases from 25 ~~°C~~ to ~~−20 °C.~~−20 °C. Lowering the temperature would decrease the diffusing ability of ~~the~~ solvent molecules. As a result, the interaction between polymer chains and solvent molecules was ~~low~~low, and thus the motion ability of amorphous PET chains was not enough to rearrange and crystallinity was limited, which ~~leaded~~led to little surface change.

3.2~~.~~. Residual ~~solvent~~Solvent of ~~electrospun~~Electrospun rPET ~~fibers~~Fibers

Figure 5a ~~presented~~ presents the FT-IR curves for electrospun PET fibers and ~~Coca-cola~~ Coca-Cola bottle pieces. For ~~Coca-Cola~~a Coca-Cola bottle sample, all characteristic peaks of function groups can be clearly observed, including terephthalic acid ester C5O at 1711 cm$^{~~-1~~-1}$, asymmetric ~~-C-C-O-~~–C–C–O– at 1238 cm$^{~~-1~~-1}$, stretching ~~-O-C-C-~~–O–C–C– at 1092 cm$^{~~-1~~-1}$, and ~~-CH-~~–CH– at 721 cm$^{~~-1~~-1}$.[30] The peaks of electrospun PET fibers moved ~~towards~~ toward a higher wavenumber, but the main peaks of two FT-IR group were similar, which indicates ~~the~~that PET did not decompose during electrospinning.

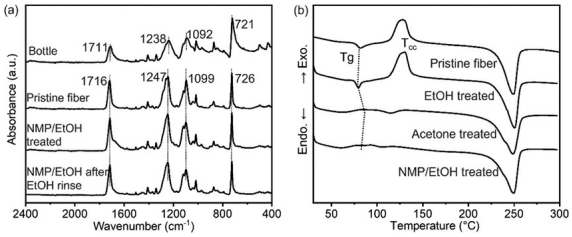

5~~.~~. (a) FTIR ~~for Coca-Cola~~spectra of Coca-Cola bottle pieces, electrospun rPET fibers before and after ~~solvents~~solvent treatment. (b) DSC traces ~~for~~of electrospun rPET fibers before and after treatment ~~of~~with different solvents for 30 min.

Due to the intensive interaction between PET and NMP, NMP ~~need~~needs to be extracted from the PET fibrous membranes after immersing in the mixture of NMP and ethanol. ~~Regarding~~Because the evaporation rate of NMP at room temperature is relatively low, the specimens ~~were~~ treated by NMP should be examined to determine whether the solvent has been removed successfully. If the membranes after immersing in ~~the~~ NMP/ethanol were dried at room temperature without further processing, NMP would be trapped among the PET fibers due to its low evaporation rate. The ~~swollen~~swelling and ~~re-crystallization~~recrystallization of PET fibers induced by NMP would happen continuously during this period. It can be seen on the FTIR curve for ~~NMP/ethanol-treated~~ NMP/ethanol-treated PET fibers without ethanol ~~rinse~~rinsing that the peak at 1683 cm$^{~~-1~~-1}$ was absent. This peak should be assigned to the C5O bond of ~~-N-C~~the –N–C5O group.[31] After ~~a twice~~rinsing with ethanol ~~rinsing, of the NMP/ethanol-treated~~ twice, NMP/ethanol-treated PET fibers disappeared. ~~It~~This indicated that the NMP trapped in the fibers ~~were~~was removed successfully. The changes of the peak at 1683 cm$^{~~-1~~-1}$ may be attributed to two reasons. One is that there was no bond formed between NMP molecules and PET polymer chains during immersion. The other is that NMP was soluble in ethanol, and therefore ~~the~~ ethanol immersion among PET fibers accelerated NMP evaporation.

3.3. Thermal–Physical Properties of PET Bottles and Electrospun rPET Fibers

Figure 5b shows DSC traces for electrospun PET fibers before and after treatment with different solvents for 30 min at room temperature. For pristine electrospun PET fibers, there were three major peaks: the glass-transition area (T_g, 81.7 °C), cold crystallization peak (T_{cc}, 128.9 °C), and melting peak (249.7 °C).

The DSC trace for electrospun fibers after ethanol treatment for 30 min was similar to the specimen of pristine PET fibers. This indicated that ethanol treatment for 30 min did not change the thermal–physical properties (Table S2) of the electrospun rPET fibers, which means that no solvent-induced recrystallization occurred during ethanol immersion. This DSC result is consistent with the SEM images, which demonstrated that the ethanol-treated fiber had a similar surface morphology to pristine fibers. By contrast, when PET fibers were immersed in acetone or NMP/ethanol solutions, these kinds of solutions can permeate into PET fibers and act as a plasticizer, which can reduce the T_g values of PET fibers, as shown in Figure 5b. The solvent-induced crystallization could be observed from the small area of the crystallization peaks as indicated by the dashed line in NMP ethanol and acetone curves.[28] The crystallization of PET fibers during immersion in NMP/ethanol showing a near-complete disappearance of cold crystallization peak indicated that some amorphous molecular chains became crystalline. Additionally, the PET fiber after acetone or NMP/ethanol treatment showed a pre-melting peak between 100 °C and 125 °C and a major melting peak at around 250 °C. In their main melting areas, there were two endotherms. The first endotherm reflected the melting behavior of crystallinities of the PET, while the second endotherms reflected the melting behavior of secondary crystallization of the PET during the heating process of DSC.[32]

3.4. Relative Crystalline Index of Electrospun rPET Fibers

The Figure 6a shows the XRD patterns of pristine electrospun PET fibers and the fibers after different solvent treatments. The Coca-Cola bottle specimen had a peak at 25.4° in Figure S1. The pristine electrospun rPET fibers showed a slight halo around 18°. Compared with the XRD patterns of the Coca-Cola bottle, the pristine electrospun fibers improved the amorphous part of raw PET material because the polymer chains consolidated before crystallization due to rapid evaporation of solvents during electrospinning.

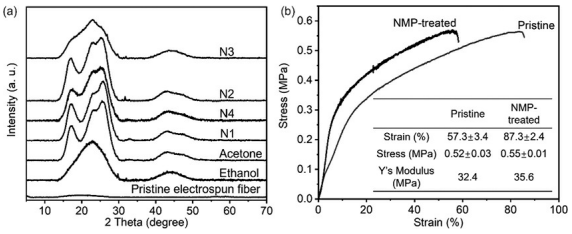

6. (a) XRD patterns for pristine and post-treated electrospun PET fibers. (b) Stress–strain curves for pristine and NMP-treated rPET fibrous membrane and their mechanical properties.

The samples E and N3, which were post-treated by ethanol treatment and NMP/ethanol (25/75, w/w), did not show crystalline peaks. They only had two amorphous peaks at around 17° and 22°. It indicated that samples E and N3 had similar structures of the amorphous phase. By contrast, sample N1 treated by NMP/ethanol (50/50, w/w) had crystalline peaks at 19.3° (010), 21.3° ($1\bar{1}$...11), 21.3° ($\bar{1}11$), and 23.1° ($1\bar{1}$...10) 23.1° ($\bar{1}10$) and two amorphous peaks. The peak at 23.1° was absent in sample N4, which was treated by NMP/ethanol (50/50, w/w) at a lower temperature (−20 °C). It (−20 °C). This means that the same solvent system after treatment at different temperatures could not affect the PET crystal structure but changed the amount of crystalline. crystal. The sample N2 that treated by NMP/ethanol (37.5/62.5, w/w) only had a crystalline peak at 22.39°. It 22.39°. This might be attributed to the fact that the positions of other two crystalline peaks were unable to resolve due to the low crystallinity.

The acetone-treated acetone-treated sample A had two amorphous peaks at 16.8° 16.8 and 25.8°. 25.8°. The difference of amorphous peaks between samples treated with acetone and NMP might be caused by the different amorphous structures of samples after

different solvent ~~treatment.~~treatments.

Separation of the amorphous peaks and crystalline peaks in the XRD patterns was ~~used~~performed to calculate the crystallinity degree for PET fibers after solvent post-treatment. The crystallinity degree for fibers after solvent treatments ~~were~~was calculated by the formula ~~(1):~~(1)

$$CI_{\text{relative crystallinity index}} = \frac{\text{total area of crystalline peaks}}{\text{total area of all peaks}} \times 100\% \quad (1)$$

The protocols to separate the amorphous and crystalline peaks in the XRD patterns of PET fibers were introduced by ~~the work of~~ Murthy ~~*et al.*~~et al.[33] The model used in the current work was model E, which involves height, ~~position~~position, and full width at ~~half maximum~~ half-maximum (FWHM). The amorphous peaks would be defined from the XRD patterns through applying the amorphous peak parameters from the template, which were used as starting values. ~~Then~~Then, the crystalline peaks would be added in profile analysis of the scans and the parameters of the amorphous peaks would be adjusted to fit the XRD patterns of PET fibers. The two reference amorphous peaks in the PET fibers are located ~~in 16.62°~~at 16.62 and ~~20.04°~~20.04°, whose ~~FWHM~~FWHMs correspond to ~~4.55°~~4.55 and ~~7.15°~~.7.15°.[33] The FWHM for crystalline peak resolved from the XRD ~~need to~~should be below ~~3°~~.3°. The background for every sample was subtracted from the XRD scans before profile analysis. The diffraction diagrams with fitted peaks are shown in ~~the~~ Figure 6a. The calculated relative ~~crystallinity is~~crystallinities are shown in ~~the~~ Table 3.

3~~.~~.

Relative ~~crystallinities for Coca-Cola bottles~~ Crystallinities of Coca-Cola Bottles and ~~electrospun~~Electrospun rPET ~~fibers~~Fibers before and after ~~different solvent treatments.~~Different Solvent Treatments

~~Sample~~ sample	~~Bottle~~ bottle	~~Pristine fiber~~ pristine fiber	~~Acetone (A)~~ acetone (A)	~~Ethanol (E)~~ ethanol (E)	~~NMP/ethanol~~NMP/ethanol ~~(w/w)~~(w/w) ~~50/50~~50/50 (N1)	~~50/50~~50/50 (N4)	~~37.5/62.5~~37.5/62.5 (N2)	~~25/75~~25/75 (N3)
CI (%)	55.5	0	52.9	0	30.5	25.3	9.7	0

When PET fibrous membranes were immersed in the solvent, the interaction between polymer chains and solvent molecular increased the motion ability of polymer ~~chains~~chains, and ~~made it possible that~~ thus polymer chains rearrange below ~~glass transition~~the glass-transition temperature, which ~~result~~ finally results in ~~the formation of crystallization finally.~~ crystallization. Due to the crystallization, ~~the~~ phase separation happened and formed ~~solvent rich~~ solvent-rich phase and ~~solvent poor~~ solvent-poor phase. After the solvent in the ~~solvent rich~~ solvent-rich phase evaporated, the porous structure of electrospun rPET fibers appeared. Compared with the similar mechanism study on ~~poly(L-lactic~~poly(l-lactic acid),[9,19] the ~~NMP induced re-crystallized~~ NMP-induced recrystallized PET fibers did not have a significant increase ~~of~~in crystallinity. Combining with the SEM images in Figure 4, it could be assumed ~~the~~that crystallization ~~that~~ induced by NMP cannot penetrate deep into the fiber ~~interior,~~interior but only occurs on the ~~fibers'~~fibers' surface. The crystallization of PET during immersion in the solvents could be verified by the disappearance (or decrease) of cold crystallization peak of DSC scanning and change of XRD diagram for electrospun rPET fibers after solvent treatments, compared with pristine electrospun PET fibers. The difference between ~~morphology~~ the morphologies of fibers treated with different solvents could be attributed to the difference between the solubility parameter of solvents and that of PET. The relatively small difference in the solubility parameter would induce larger morphological modification.

The changes ~~of~~ in the mechanical performances between pristine and NMP-treated (N1) samples ~~was~~are presented in Figure 6b. The amorphous pristine electrospun rPET is elastic. ~~Comparing~~Compared with the pristine membrane, the NMP-treated membrane showed higher stress and ~~Young's modulus~~Young's modulus, while its elongation at ~~the breaking point~~ break was reduced significantly. This change consists ~~with~~of the increased crystallinity with ~~the solvent induced re-crystallization.~~solvent-induced recrystallization.

3.5~~.~~. Air ~~filtration performance evaluation~~Filtration Performance Evaluation

3.5.1~~.~~. PM2.5 ~~aerosols filtration~~Aerosol Filtration

Figure 7 demonstrates the air filtration performances of pristine and NMP post-treated electrospun rPET fibrous membrane samples. For both pristine and NMP post-treated membranes, three groups with different ~~thickness that~~ thicknesses controlled by setting different electrospinning ~~time~~times were examined. The ~~1h~~ 1 h sample was the thinnest ~~one~~one, whereas the 3 h sample was the thickest. Contrary to expectation, the results show that the pristine membranes have better filtration speed than the NMP post-treated ones and the thinner

membranes are better than the thicker ones.

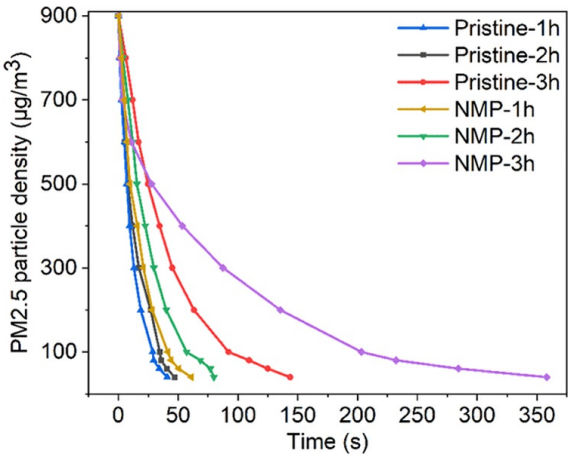

7~~.~~. ~~The filtration~~ Filtration time for membrane to reduce PM2.5 from 900 to 40 ~~μg/m~~μg/m^3. The membrane thickness increases with ~~the~~a longer spinning time from 1 ~~h~~ to 3 h.

PM2.5 is the major air pollution concern that industrialized society ~~need~~needs to face. As a typical kind of aerosol pollutant, the threat of PM2.5 to the human body is obvious, especially aerosols have been recognized as the primary transmission route for the spread of COVID-19 during the pandemic from 2020 till now.[34,35] Despite ~~of~~ varieties of face masks, fibrous membranes have been also widely applied in other fields ~~range~~ranging from industry to domestic.[36]

The performance parameters between PPE masks and ~~industrial/ domestic~~ industrial/domestic systems are different. This is mainly due to the ~~airflow~~ air flow flux of human ~~breathing~~breathing, and fresh air filtration equipment often differs by more than an order of magnitude.[37] As a result, the aerosol filtration mechanisms ~~that~~in PPE masks and industrial/domestic systems rely on completely different mechanisms. In particular, the air flow from human breath is a laminar ~~flow~~flow, which could induce the aerosol particles ~~moves~~ to move regularly. The major filtration mechanisms of fibrous membrane including interception and impaction could only happen under the scenario of laminar flow. However, the aerosol ~~particles~~particles' air flow generated by the brushless duct motor is ~~pretty~~ fast. ~~The flowing eq~~Eq 2 could be used to identify the situation of air flow at the duct ~~motor:~~motor

$$\mathrm{Re} = \frac{\rho v d}{\eta} \quad 2$$

~~Where ρ~~where ρ is the air density (1.225 kg/m^3); *v* is the air flow ~~speed~~speed, which is 3 m/s in this work; and *d* is the dynamic viscosity of 1.81 ~~×~~× 10~~$^{-5}$~~$^{-5}$ ~~Pa·s.~~Pa·s. It could be calculated that the Reynolds number of air flow at the duct motor is about ~~10,000~~10000, which is a typical turbulent flow. But the air flow mechanism in porous materials has not been a consensus yet.[38] Referring to the rPET fibrous membrane in this work, the solvent post-treatment process would not only change the ~~fibers'~~fibers' surface morphology but also make the fibrous membrane more compact. This change ~~attribute~~attributes to the lower air permeability or pressure drop of post-treated membranes than that of the pristine ones. Thus, for the same fibrous membrane samples before and after post-treatment, the sample without treatment has a high air flux and consequently faster filtration efficiency.

Due to the relatively ~~fine~~low diameter of PET fibers and the small interior space among fibers, most ~~of~~ aerosol particles were trapped on the surface of membrane filter (Figure S3). The fast sacked particles would ~~from~~form a filter cake,[39] which could ~~elevate~~increase the filtration efficiency rapidly, especially under a large flux air flow. Thus, the thicker membrane would be not suitable for face masks due to its higher pressure drop. The video of aerosol filtration process (Supporting ~~video~~Video 01) recorded the fast ~~accumulated~~accumulation on the surface of rPET fibrous ~~membrane~~membrane, which could prove this mechanism. A ~~longer time~~ longer-term filtration test demonstrated the stability of this membrane in the same video.[40]

3.5.2~~.~~. Fluorescent ~~protein mimicking virus filtration~~Protein Mimicking Virus Filtration

Viruses, including SARS-COV-2 coronavirus, which has caused a pandemic in the past one and a half years, are essentially ~~sub-micron~~submicron protein macromolecules.[41] Extensive studies have confirmed that human body fluids the containing SARS-COV-2 virus are the main way to spread COVID-19.[42] Moreover, this fact has been recognized and taken into policies by ~~the~~ governments all over the

world.[43,44] Considering the risk of virus handling, this experiment uses the fluorescent protein mimic virus commonly used in biological laboratories to test the performance of the virus-containing water mist filtration of the rPET fibrous membrane.[22,45] This study uses an atomization device to disperse the fluorescent protein solution of appropriate concentration into small droplets, which simulates ~~the~~ human body fluids such as those from coughing or sneezing to spread the virus (Supporting ~~video~~Video 02). As shown in Figure 2b, the experiment used an external air flow to guide the water ~~mist-containing~~ mist-containing fluorescent protein to pass through the fibrous membrane filter. After filtration tests, a ~~fluorescent~~fluorescence microscope was used to observe the residual fluorescent protein on the surface of membrane filters and the receiving plates (cultivation dishes) installed behind the fan. If most of the protein particles remain on the surface of the fiber membrane and there is almost no fluorescent protein on the ~~petri~~Petri dish, ~~it means~~ the surface of the testing sample retains most of the contaminants and ~~has~~shows good filtering performance, and vice versa.

Figure 8 presents the results of the above experiment. The conventional three-layer ~~non-woven~~nonwoven surgical mask was involved ~~into~~in the experiment as a comparison group. Overall, rPET fibrous membrane, whether ~~it is~~ pristine or ~~NMP-treated,~~ NMP-treated, has ~~achieved~~shown good results ~~comparable~~compared to the second layer of the mask. The second layer is the vital layer that applies the electret technology in surgical masks to intercept pollutants. On the surface of the second layer of PET membrane samples and surgical masks, it was obviously observed that a large number of fluorescent protein particles are attached to the fiber surface. The third layer of surgical masks is mainly a layer that plays a role of moisture absorption in commercial design.[37] The third layer of surgical ~~mask~~masks has almost no interception effect of fluorescent protein. By observing the surface of the ~~petri~~Petri dish behind the ducted fan, we could conclude that the third layer of the surgical mask cannot filter most protein particles. Although the second layer of the surgical mask has a good filtering efficiency, some fibers were detached from the surface of the membrane due to continuous ~~airflow,~~ air flow, while some fluorescent proteins are carried along with these fibers. This result proves that the melt-blown electret filter membrane cannot be used as a safe virus protection device alone but needs the assistance of the back layer of ~~non-woven~~nonwoven fabric. On the contrary, the rPET fibrous membranes fabricated by electrospinning are more stable in the working environment. These electrospun membranes not only can effectively intercept the virus, but also the membrane itself was not damaged. Further comparison shows that fewer fluorescent proteins can be passed through the ~~NMP-treated~~ NMP-treated sample. Therefore, the filtering capability of post-treated ~~high-roughness~~ high-roughness fibrous membrane is better. This may be attributed to its rougher ~~fibers'~~fiber surface, which ~~leads to~~ gives the membrane more opportunities for interception.

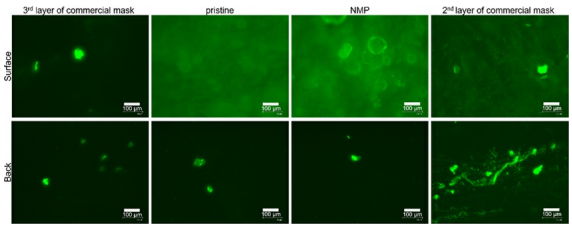

8~~.~~. ~~The microscope~~ Microscope images of fluorescent proteins mimicking virus ~~which~~that were captured on the surface of membrane filter and left on receiving ~~petri~~Petri dish.

4~~.~~. Conclusions

In brief, the rPET fibers and fibrous membranes were successfully electrospun by applying TFA/DCM (50/50, w/w) in this work. Observed by SEM images, the hypothesis of controlling ~~PET fibers~~ the surface morphology of PET fibers by adjusting post-treatment parameters was proved. It can be found that either NMP or acetone under appropriate conditions can generate obvious porous structure on the surface of rPET fibers. It was confirmed by further characterization that the ~~morphology~~morphological change of electrospun rPET fibers was attributed to ~~solvent-induced~~the solvent-induced crystallization mechanism. The pristine PET membranes could filter PM2.5 aerosol ~~particles~~particles, but the NMP post-treated membrane shows ~~the~~ better filtration capability for ~~proteins~~protein capturing. Therefore, the electrospun rPET fibrous membrane developed in this work can be applied ~~to~~for the effective filtration of various pollutants including PM2.5 and viruses and is especially suitable for potential applications in industrial or domestic ~~high-flux~~ high-flux filtration equipment.

Supporting information

The Supporting Information is available free of charge at https://pubs.acs.org/doi/10.1021/acsami.xxxxxxx.

~~The thickness~~ Thickness of rPET fibrous membranes for aerosol filtration; ~~Thermo~~thermal properties of PET bottle, pristine and post-treated rPET fibrous membranes; ~~The~~ optical photo of internal air flow for PM2.5 aerosol capturing and virus interception air filtration test; and SEM image of rPET fibrous membrane after aerosol filtration ~~test; and The videos of PM2.5 aerosol capturing and virus interception air filtration experiments.~~ test (PDF)

Videos of PM2.5 aerosol capturing and virus interception air filtration experiments (MP4)

(MP4)

The ~~3D printed~~ 3D-printed model (Shapr3D) used in this ~~manuscript~~study is freely available at: https://github.com/Airslashcn/3D-printing-for-aerosol-filtration.

Acknowledgments

This ~~research~~study was a part of the project ~~"Improved~~"Improved face-worn PPE designs for use by the public and professionals to reduce audio-visual communication ~~difficulties~~"difficulties", which was supported by EPSRC (EP/V051571/1).

The authors ~~thank for~~ acknowledge the support of the Electron Microscopy Centre and XRD suite in Department of Materials, The University of Manchester. ~~Jun Song~~ J.S. and ~~Zhongda Chen~~ Z.C. acknowledge the technical support from Luis Larrea Murillo in Division of Evolution and Genomic Sciences, The University of Manchester.

References

1Kemfert C. ~~'Climate Neutral'~~'Climate Neutral' Is a Lie — Abandon It as a Goal Nature 2021 591 7848 34 34 10.1038/d41586-021-00543-9.

2Net-Zero Carbon Pledges Must Be Meaningful to Avert Climate Disaster. Nature 2021, 592 ~~(~~7852~~),~~ 8 8. 10.1038/d41586-021-00864-9.

3Wang Z. Sedighi M. Lea-Langton A. Filtration of Microplastic Spheres by Biochar: Removal Efficiency and Immobilisation Mechanisms Water Res. 2020 184 116165 10.1016/j.watres.2020.116165.

4Azmin, S. N. H. M. ~~binti M.~~ ; Hayat, N. A. ~~binti M.~~ ; ; Nor, M. S. M. Development and Characterization of Food Packaging Bioplastic Film from Cocoa Pod Husk Cellulose Incorporated with Sugarcane Bagasse Fibre, J. Bioresour. Bioprod. 2020, 5 4 248 255, 10.1016/j.jobab.2020.10.003.

5Hao J. Passos de Oliveira Santos R. Rutledge G. C. Examination of Nanoparticle Filtration by Filtering Facepiece Respirators During the COVID-19 Pandemic ACS Appl. Nano Mater. 2021 4 4 3675 3685 10.1021/acsanm.1c00139.

6Jiang X. Bai Y. Chen X. Liu W. A Review on Raw Materials, Commercial Production and Properties of Lyocell Fiber J. Bioresour. Bioprod. 2020 5 1 16 25 10.1016/j.jobab.2020.03.002.

7Song J. Chen Z. Murillo L. L. Tang D. Meng C. Zhong X. Wang T. Li J. Hierarchical Porous Silk Fibroin/Poly(L-Lactic Acid) Fibrous Membranes towards Vascular Scaffolds Int. J. Biol. Macromol. 2021 166 1111 1120 10.1016/j.ijbiomac.2020.10.266.

8Zia Q. Tabassum M. Meng J. Xin Z. Gong H. Li J. Polydopamine-Assisted Grafting of Chitosan on Porous Poly (L-Lactic Acid) Electrospun Membranes for Adsorption of Heavy Metal Ions Int. J. Biol. Macromol. 2021 167 1479 1490 10.1016/j.ijbiomac.2020.11.101.

9Song, J.; Zhang, B.; Lu, Z.; Xin, Z.; Liu, T.; Wei, W.; Zia, Q.; Pan, K.; Gong, R. H.; Bian, L.; Li, Y.; Li, J. Hierarchical Porous Poly(l -Lactic Acid) Nanofibrous Membrane for Ultrafine Particulate Aerosol Filtration. ACS Appl. Mater. Interfaces 2019, 11 ~~(~~49~~).~~ 46261. 10.1021/acsami.9b18083.

10Wang F. Dai J. Huang L. Si Y. Yu J. Ding B. Biomimetic and Superelastic Silica Nanofibrous Aerogels with Rechargeable Bactericidal Function for Antifouling Water Disinfection ACS Nano 2020 14 7 8975 8984 10.1021/acsnano.0c03793.

11Crilley- L. R.- Angelucci- A. A.- Malile- B.- Young- C. J.- VandenBoer- T. C.- Chen- J. I. L.- Non-Woven Materials for Cloth-Based Face Masks Inserts: Relationship between Material Properties and Sub-Micron Aerosol Filtration—— Environ. Sci. Nano- 2021- 8- 6- 1603- 1613- 10.1039/D1EN00277E.

12Yue- Y.- Gong- X.- Jiao- W.- Li- Y.- Yin- X.- Si- Y.- Yu- J.- Ding- B.- In-Situ Electrospinning of Thymol-Loaded Polyurethane Fibrous Membranes for Waterproof, Breathable, and Antibacterial Wound Dressing Application—— J. Colloid Interface Sci.- 2021- 592- 310- 318- 10.1016/j.jcis.2021.02.048.

13Huang— C.— Thomas— N. L.— Fabrication of Porous Fibers via Electrospinning: Strategies and Applications— Polym. Rev.- 2019- 1- 53- 10.1080/15583724.2019.1688830.

14Laity- P.- Glover- P.- Hay- J.- Composition and Phase Changes Observed by Magnetic Resonance Imaging during Non-Solvent Induced Coagulation of Cellulose- Polymer ~~(Guildf)~~ 2002- 43- 22- 5827- 5837- 10.1016/S0032-3861(02)00531-1.

15Strain- I. N.- Wu- Q.- Pourrahimi- A. M.- Hedenqvist- M. S.- Olsson- R. T.- Andersson- R. L.- Electrospinning of Recycled PET to Generate Tough Mesomorphic Fibre Membranes for Smoke Filtration- J. Mater. Chem. A- 2015- 3- 4- 1632- 1640- 10.1039/C4TA06191H.

16Bonfim- D. P. F.- Cruz- F. G. S.- Bretas- R. E. S.- Guerra- V. G.- Aguiar- M. L.- A Sustainable Recycling Alternative: Electrospun PET-Membranes for Air Nanofiltration- Polymers ~~(Basel)~~ 2021- 13- 7- 1166- 10.3390/polym13071166.

17de Oliveira Santos- R. P.- Rodrigues- B. V. M.- Santos- D. M. dos- Campana-Filho- S. P.- Ruvolo-Filho- A. C.- Frollini- E.- Electrospun Recycled PET-Based Mats: Tuning the Properties by Addition of Cellulose and/or Lignin—— Polym. Test- 2017- 60- 422- 431- 10.1016/j.polymertesting.2017.04.023.

18Shu- D.- Xi- P.- Li- S.- Li- C.- Wang- X.- Cheng- B.- Morphologies and Properties of PET Nano Porous Luminescence Fiber: Oil Absorption and Fluorescence-Indicating Functions- ACS Appl. Mater. Interfaces- 2018- 10- 3- 2828- 2836- 10.1021/acsami.7b16655.

19Lu— Z.— Zhang— B.— Gong— H.— Li— J.— Fabrication of Hierarchical Porous Poly (l-Lactide) (PLLA) Fibrous Membrane by Electrospinning- Polymer ~~(Guildf)~~ 2021- 226- - 123797- 10.1016/j.polymer.2021.123797.

20Awaja- F.- Pavel- D.- Recycling of PET- Eur. Polym. J.- 2005- 41- 7- 1453- 1477- 10.1016/j.eurpolymj.2005.02.005.

21Huang- X.- Jiao- T.- Liu- Q.- Zhang- L.- Zhou- J.- Li- B.- Peng- Q.- Hierarchical Electrospun Nanofibers Treated by Solvent Vapor Annealing as Air Filtration Mat for High-Efficiency PM2.5 Capture- Sci. China Mater.- 2019- 62- 3- 423- 436- 10.1007/s40843-018-9320-4.

22Rajesh- S.- Crandall- C.- Schneiderman- S.- Menkhaus- T. J.- Cellulose- Graft -Polyethyleneamidoamine Anion-Exchange Nanofiber Membranes for Simultaneous Protein Adsorption and Virus Filtration——— ACS Appl. Nano Mater.- 2018- 1- 7- 3321- 3330- 10.1021/acsanm.8b00519.

23Veleirinho- B.- Rei- M. F.- Lopes-DA-Silva- J. A.- Solvent and Concentration Effects on the Properties of Electrospun Poly(Ethylene Terephthalate) Nanofiber Mats- J. Polym. Sci. Part B Polym. Phys.- 2008- 46- 5- 460- 471- 10.1002/polb.21380.

24Barton, A. F. M. CRC Handbook of Solubility Parameters and Other Cohesion Parameters; Routledge, 2017. ~~10.1201/9781315140575.~~

25Tamizifar- M.- Sun- G.- Control of Surface Radical Graft Polymerization on Polyester Fibers by Using Hansen Solubility Parameters as a Measurement of the Affinity of Chemicals to Materials- RSC Adv.- 2017- 7- 22- 13299- 13303- 10.1039/C6RA27186C.

26Tamizifar- M.- Sun- G.- Surface Modification of Poly(Ethylene Terephthalate) Fibers via Controlled Radical Graft Polymerization- J. Appl. Polym. Sci.- 2018- 135- 11- 45990- 10.1002/app.45990.

27Moore— W. R.— Sheldon— R. P.— The Crystallization of Polyethylene Terephthalate by Organic Liquids— Polymer ~~(Guildf)~~ 1961- 2- 315- 321- 10.1016/0032-3861(61)90034-9.

28Ouyang- H.- Lee- W.-H.- Ouyang- W.- Shiue- S.-T.- Wu- T.-M.- Solvent-Induced Crystallization in Poly(Ethylene Terephthalate) during Mass Transport: Mechanism and Boundary Condition- Macromolecules- 2004- 37- 20- 7719- 7723- 10.1021/ma0400416.

29Jameel– H.– Noether– H. D.– Rebenfeld– L.– The Effects of Orientation and Crystallinity on the Solvent-Induced Crystallization of Poly(Ethylene Terephthalate). II. Physical Structure and Morphology——— J. Appl. Polym. Sci.– 1982– 27– 3– 773– 793– 10.1002/app.1982.070270301.

30Chen– Z.– Hay– J. N.– Jenkins– M. J.– FTIR Spectroscopic Analysis of Poly(Ethylene Terephthalate) on Crystallization– Eur. Polym. J.– 2012– 48– 9– 1586– 1610– 10.1016/j.eurpolymj.2012.06.006.

31Chen– Z.– Hay– J. N.– Jenkins– M. J.– The Thermal Analysis of Poly(Ethylene Terephthalate) by FTIR Spectroscopy– Thermochim. Acta– 2013– 552– 123– 130– 10.1016/j.tca.2012.11.002.

32Groeninckx– G.– Reynaers– H.– Morphology and Melting Behavior of Semicrystalline Poly(Ethylene Terephthalate). II. Annealed PET– J. Polym. Sci. Polym. Phys. Ed.– 1980– 18– 6– 1325– 1341– 10.1002/pol.1980.180180613.

33Murthy– N. S.– Minor– H.– General Procedure for Evaluating Amorphous Scattering and Crystallinity from X-Ray Diffraction Scans of Semicrystalline Polymers– Polymer ~~(Guildf)~~ 1990– 31– 6– 996– 1002– 10.1016/0032-3861(90)90243-R.

34Wang– C. C.– Prather– K. A.– Sznitman– J.– Jimenez– J. L.– Lakdawala– S. S.– Tufekci– Z.– Marr– L. C.– Airborne Transmission of Respiratory Viruses– Science ~~(80-.)~~ 2021– 373– 6558– – eabd9149– 10.1126/science.abd9149.

35Nazarenko—— Y.—— Air Filtration and Severe Acute Respiratory Syndrome Coronavirus 2—— Epidemiol. Health– 2020– – e2020049– 10.4178/epih.e2020049.

36Zhang—— R.—— Liu—— B.—— Yang—— A.—— Zhu—— Y.—— Liu—— C.—— Zhou—— G.—— Sun—— J.—— Hsu—— P.-C.– Zhao– W.– Lin– D.– Liu– Y.– Pei– A.– Xie– J.– Chen– W.– Xu– J.– Jin– Y.– Wu– T.– Huang– X.– Yi– C.– In Situ Investigation on the Nanoscale Capture and Evolution of Aerosols on Nanofibers– Nano Lett.– 2018– 18– 2– 1130– 1138– 10.1021/acs.nanolett.7b04673.

37Liu– J.– Zhang– H.– Gong– H.– Zhang– X.– Wang– Y.– Jin– X.– Polyethylene/Polypropylene Bicomponent Spunbond Air Filtration Materials Containing Magnesium Stearate for Efficient Fine Particle Capture——— ACS Appl. Mater. Interfaces– 2019– 11– 43– 40592– 40601– 10.1021/acsami.9b13162.

38Jin– Y.– Uth– M.-F.– Kuznetsov– A. V.– Herwig– H.– Numerical Investigation of the Possibility of Macroscopic Turbulence in Porous Media: A Direct Numerical Simulation Study– J. Fluid Mech.– 2015– 766– 76– 103– 10.1017/jfm.2015.9.

39Bai– H.– Qian– X.– Fan– J.– Shi– Y.– Duo– Y.– Guo– C.– Wang– X.– Theoretical Model of Single Fiber Efficiency and the Effect of Microstructure on Fibrous Filtration Performance: A Review– Ind. Eng. Chem. Res.– 2021– 60– 1– 3– 36– 10.1021/acs.iecr.0c04400.

40Lv– D.– Tang– G.– Chen– L.– Zhang– M.– Cui– J.– Xiong– R.– Huang– C.– Multifunctional Gas-Spinning Hierarchical Architecture: A Robust and Efficient Nanofiber Membrane for Simultaneous Air and Water Contaminant Remediation—— ACS Appl. Polym. Mater.– 2020– 2– 12– 5686– 5697– 10.1021/acsapm.0c00988.

41Bar-On, Y. M.; Flamholz, A.; Phillips, R.; Milo, R. SARS-CoV-2 (COVID-19) by the Numbers. Elife 2020, 9, e57309. 10.7554/eLife.57309.

42Sousan– S.– Garcia– N.– White– A.– Balanay– J. A.– Filtration Efficiency of Surgical Sterilization Fabric for Respiratory Protection during COVID-19 Pandemic– Am. J. Infect. Control– 2021– 49– 1– 1– 7– 10.1016/j.ajic.2020.11.005.

43Guo– Z.-D.– Wang– Z.-Y.– Zhang– S.-F.– Li– X.– Li– L.– Li– C.– Cui– Y.– Fu– R.-B.– Dong– Y.-Z.– Chi– X.-Y.– Zhang– M.-Y.– Liu– K.– Cao– C.– Liu– B.– Zhang– K.– Gao– Y.-W.– Lu– B.– Chen– W.– Aerosol and Surface Distribution of Severe Acute Respiratory Syndrome Coronavirus 2 in Hospital Wards, Wuhan, China, 2020– Emerg. Infect. Dis.– 2020– 26– 7– 1583– 1591– 10.3201/eid2607.200885.

44Mittal– R.– Ni– R.– Seo– J.-H.– The Flow Physics of COVID-19– J. Fluid Mech.– 2020– 894– F2– 10.1017/jfm.2020.330.

45Beesoon– S.– Behary– N.– Perwuelz– A.– Universal Masking during COVID-19 Pandemic: Can Textile Engineering Help Public Health? Narrative Review of the Evidence– Prev. Med. ~~(Baltim)~~ 2020– 139– – 106236– 10.1016/j.ypmed.2020.106236.